B. V. Carlson · R. Capote · M. Sin

Elastic and inelastic breakup of deuterons with energy below 100 MeV

Abstract We present calculations of deuteron elastic and inelastic breakup cross sections and angular distributions at deuteron energies below 100 MeV obtained using the post-form DWBA approximation. The elastic breakup cross section was extensively studied in the past. Very few calculations of inelastic breakup have been performed, however. We also analyze the angular momentum - energy distributions of the cross section for formation of the compound nucleus after inelastic breakup.

1 Introduction

Deuteron-induced reactions are being used to produce medical radioisotopes [1] and as surrogates to other reactions (see review [2] and references therein), among recent applications. Although they have been studied for decades [3; 4; 5; 6], the complexity of these reactions continues to make their theoretical description challenging.

The direct reaction mechanism is a major contributor to the deuteron reaction cross section due to the particle's low binding energy. . Competition between elastic breakup, absorption of only a neutron or a proton (stripping and inelastic breakup) and absorption of the deuteron must be taken into account to determine the formation or not of a compound nucleus and its subsequent decay. The inelastic breakup reactions - those in which either only a neutron or a proton is absorbed - are particularly complex, as they form compound nuclei with a wide range of excitation energies and angular momenta. We present the results of a theoretical study of elastic and inelastic deuteron breakup for a large selection of targets at incident deuteron energies below 100 MeV. We use the zero-range post-form DWBA approximation to calculate the elastic breakup cross section [3; 4] and its extension to absorption channels to calculate the inelastic breakup cross sections [5; 6]. We discuss the regularities and ambiguities in our results, as well as the irregularities in the inelastic breakup energy and angular momentum distributions that complicate their substitution by a smooth distribution obtained from systematics.

B. V. Carlson
Instituto Tecnológico de Aeronáutica, São José dos Campos SP, Brazil
E-mail: brett@ita.br

R. Capote
NAPC-Nuclear Data Section, International Atomic Energy Agency, 1400 Vienna, Austria

M. Sin
University of Bucharest, P.O. Box MG-11, 70709 Bucharest-Magurele, Romania

2 Theory

A reasonable theoretical description of elastic deuteron breakup was developed and applied to a multitude of experimental data almost forty years ago by G. Baur and collaborators [3; 4]. The double-differential inelastic breakup cross section can be written in terms of its T-matrix element as

$$\frac{d^6\sigma^{bu}}{dk_p^3 dk_n^3} = \frac{2\pi}{\hbar v_d}\frac{1}{(2\pi)^6}\left|T(\mathbf{k}_p,\mathbf{k}_n;\mathbf{k}_d)\right|^2\delta(E_d+\varepsilon_d-E_p-E_n) \tag{1}$$

where $\mathbf{k}_n$ and $\mathbf{k}_p$ are the final neutron and proton momenta, respectively, $\mathbf{k}_d$ is the initial deuteron momentum and the sum of neutron and proton final kinetic energies is constrained to the sum of the initial deuteron kinetic energy and its binding energy by the δ-function. The T-matrix element can be well approximated by the post-form of the DWBA matrix element,

$$T(\mathbf{k}_p,\mathbf{k}_n;\mathbf{k}_d) = \left\langle \tilde{\psi}_p^{(-)}(\mathbf{k}_p,\mathbf{r}_p)\tilde{\psi}_n^{(-)}(\mathbf{k}_n,\mathbf{r}_n)\left|v_{pn}(\mathbf{r})\right|\psi_d^{(+)}(\mathbf{k}_d,\mathbf{R})\phi_d(\mathbf{r})\right\rangle , \tag{2}$$

which, in turn, can be well-approximated within the zero-range DWBA approximation

$$T(\mathbf{k}_p,\mathbf{k}_n;\mathbf{k}_d) \rightarrow D_0 \left\langle \tilde{\psi}_p^{(-)}(\mathbf{k}_p,a\mathbf{R})\tilde{\psi}_n^{(-)}(\mathbf{k}_n,\mathbf{R})\Lambda(R)\,\middle|\,\psi_d^{(+)}(\mathbf{k}_d,\mathbf{R})\right\rangle \tag{3}$$

by including a correction for finite-range effects $\Lambda(R)$ [7] and taking $D_0 =$-125 Mev-fm$^{3/2}$.

To calculate the inelastic breakup cross section, one first analyzes the inclusive double differential breakup cross section, here given for the proton, again in the post-form of the DWBA. The initial state of the target is its ground state, Φ_A, but the final neutron-target state, ψ_{nA}^c, can be any composite state allowed by energy and angular momentum conservation,

$$\frac{d^3\sigma}{dk_p^3} = \frac{2\pi}{\hbar v_d}\frac{1}{(2\pi)^3}\sum_c\left|\left\langle \tilde{\psi}_p^{(-)}(\mathbf{k}_p,\mathbf{r}_p)\psi_{nA}^c\left|v_{pn}(\mathbf{r})\right|\psi_d^{(+)}(\mathbf{k}_d,\mathbf{R})\phi_d(\mathbf{r})\Phi_A\right\rangle\right|^2\delta(E_d+\varepsilon_d-E_p-E_{nA}^c). \tag{4}$$

Following Kasano and Ichimura [5], we write the δ-function as the imaginary part of an energy denominator,

$$\frac{d^3\sigma}{dk_p^3} = -\frac{2}{\hbar v_d}\frac{1}{(2\pi)^3}\text{Im}\sum_c\left\langle \psi_d^{(+)}\phi_d\Phi_A\left|v_{pn}\right|\tilde{\psi}_p^{(-)}\psi_{nA}^c\right\rangle \tag{5}$$

$$\times\left(E_d^+ +\varepsilon_d-E_p-E_{nA}^c\right)^{-1}\left\langle \tilde{\psi}_p^{(-)}\psi_{nA}^c\left|v_{pn}\right|\psi_d^{(+)}\phi_d\Phi_A\right\rangle ,$$

the target ground-state matrix element of which we interpret as a neutron optical propagator,

$$G_n^{(+)}(E_d+\varepsilon_d-E_p) = \sum_c\left(\Phi_A\left|\psi_{nA}^c\right\rangle\frac{1}{E_d^+ +\varepsilon_d-E_p-E_{nA}^c}\left\langle\psi_{nA}^c\right|\Phi_A\right).$$

This furnishes a cross section of the form

$$\frac{d^3\sigma}{dk_p^3} = -\frac{2}{\hbar v_d}\frac{1}{(2\pi)^3}\text{Im}\left\langle \chi_n(\mathbf{r}_n)\left|G_n^{(+)}(E_d+\varepsilon_d-E_p)\right|\chi_n(\mathbf{r}_n)\right\rangle , \tag{6}$$

where the effective neutron wave function is given by

$$\chi_n(\mathbf{r}_n) = \left(\tilde{\psi}_p^{(-)}(\mathbf{r}_p)\left|v_{pn}(\mathbf{r})\right|\psi_d^{(+)}(\mathbf{R})\phi_d(\mathbf{r})\right). \tag{7}$$

To reduce this further, the imaginary part of the optical propagator is decomposed as

$$\text{Im}\,G_n = \left(1+G_n^\dagger U_n^\dagger\right)\text{Im}\,G_0\left(1+U_nG_n\right)+G_n^\dagger W_nG_n. \tag{8}$$

The inclusive proton emission cross section from breakup can then be separated into an elastic and inelastic part, denoted here by *bu* for elastic breakup and *bf* for inelastic breakup or breakup-fusion, corresponding to the first and second terms of the decompositon of the propagator, respectively,

$$\frac{d^3\sigma}{dk_p^3} = \frac{d^3\sigma^{bu}}{dk_p^3} + \frac{d^3\sigma^{bf}}{dk_p^3}.$$ (9)

The contribution due to elastic breakup

$$\frac{d^3\sigma^{bu}}{dk_p^3} = \frac{2\pi}{\hbar v_d}\frac{1}{(2\pi)^3}\int\frac{d^3k_n}{(2\pi)^3}\left|T(\mathbf{k}_p,\mathbf{k}_n;\mathbf{k}_d)\right|^2\delta(E_d+\varepsilon_d-E_p-E_n),$$ (10)

is just the double differential cross section of Eq. (1) integrated over the neutron momentum. The inelastic breakup cross section takes the form of an expectation value of the imaginary part of the optical potential,

$$\frac{d^3\sigma^{bf}}{dk_p^3} = -\frac{2}{\hbar v_d}\frac{1}{(2\pi)^3}\left\langle\Psi_n(\mathbf{k}_p,\mathbf{r}_n;\mathbf{k}_d)\right|W_n(\mathbf{r}_n)\left|\Psi_n(\mathbf{k}_p,\mathbf{r}_n;\mathbf{k}_d)\right\rangle,$$ (11)

where the effective neutron wave function is given by

$$\left|\Psi_n(\mathbf{k}_p,\mathbf{r}_n;\mathbf{k}_d)\right\rangle = \left(\tilde{\psi}_p^{(-)}(\mathbf{k}_p,\mathbf{r}_p)G_n^{(+)}\left(\mathbf{r}_n,\mathbf{r}_n'\right)\left|v_{pn}(\mathbf{r})\right|\psi_d^{(+)}(\mathbf{k}_d,\mathbf{R})\phi_d(\mathbf{r})\right).$$ (12)

The physical interpretation of this cross section is simple: the deuteron first breaks up and, after propagating further, the neutron is absorbed while the proton is emitted. This wave function can be well-approximated in the zero-range approximation, again including the finite range correction $\Lambda(R)$ of Ref. [7], as

$$\left|\Psi_n(\mathbf{k}_p,\mathbf{r}_n;\mathbf{k}_d)\right\rangle \rightarrow D_0\left(\tilde{\psi}_p^{(-)}(\mathbf{k}_p,a\mathbf{R})G_n^{(+)}(\mathbf{r}_n,\mathbf{R})\Lambda(R)\,|\,\psi_d^{(+)}(\mathbf{k}_d,\mathbf{R})\right).$$ (13)

To perform numerical calculations, the wave functions and matrix elements are expanded in partial waves of the orbital angular momentum alone. We thus neglect the effects of spin-orbit coupling but thereby reduce the number of matrix elements by a factor of almost 12.

To calculate the distorted wave functions, the Koning-Delaroche global optical potentials [8] were used in the proton and neutron channels while the potentials of Refs. [9] or [10] were used to describe the deuteron scattering. Both deuteron optical potentials yield very similar results. We used the potential of Ref. [9] in the calculations presented here.

The elastic breakup matrix elements of Eq. (3) are only conditionally convergent. A simple brute force application of standard integration methods requires integrating to radii of the order of a nanometer. The numerical integration can be reduced to radii of the order of picometers by using asymptotic expansions of the Coulomb wave functions to approximate the integral in the external region analytically. However, we have found the most efficient means of performing the integrals to be their extension to the complex plane as proposed by Vincent and Fortune [11]. In this case, we can usually limit the numerical integration to several hundreds of fm and could probably limit it even more, were we to invest more effort in the evaluation of the Coulomb wave functions in the complex plane.

3 Calculations

We begin by presenting calculations of neutron and proton spectra from the elastic and inelastic breakup of 30 MeV deuterons incident on ^{48}Ti and ^{181}Ta, shown in Fig. 1. In both cases, the inelastic breakup spectra are larger than the elastic ones. The elastic and inelastic spectra for neutron or proton both peak at about the same energy in both reactions with the proton spectra peaking at higher energy than the neutron ones.

The difference in the the maxima of the neutron and proton spectra in Fig. 1 can be interpreted in terms of the Coulomb deceleration of the deuteron and posterior Coulomb acceleration of the outgoing proton. At the radius at which breakup occurs, R_{bu}, we would expect the deuteron to have lost a kinetic energy of Ze^2/R_{bu},
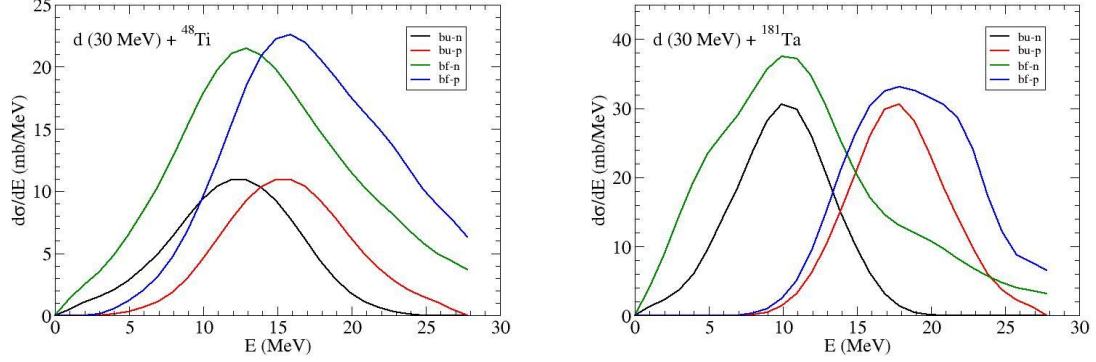
Fig. 1 (a) Proton and neutron emission spectra from elastic and inelastic breakup spectra of 30 MeV deuterons incident on ^{48}Ti. (b) Proton and neutron emission spectra from elastic and inelastic breakup spectra of 30 MeV deuterons incident on ^{181}Ta.

which is later recovered by the outgoing proton. On the average, we would thus expect to find for the outgoing neutron and proton kinetic energies

$$E_n \approx \frac{1}{2}\left(E_d - \frac{Ze^2}{R_{bu}} - \varepsilon_d\right) \tag{14}$$

$$E_p \approx \frac{1}{2}\left(E_d + \frac{Ze^2}{R_{bu}} - \varepsilon_d\right).$$

Interpreting the difference in the peaks as the energy difference at the most probable radius, we find the breakup radius R_{bu} to be 10.6 fm for ^{48}Ti and 14.6 fm for ^{181}Ta. We compare these values to strong interaction radii of 6.0 fm for ^{48}Ti and 8.6 fm for ^{181}Ta, obtained by taking $R_{int} \approx 1.25(A^{1/3} + 2^{1/3})$ fm, with A the target mass number. We conclude that the breakup occurs predominantly in the Coulomb field of the target.

In Fig. 2, we compare our calculations with the experimental inclusive double differential proton cross sections for 56 MeV deuterons incident on ^{27}Al and ^{118}Sn [12]. The cross sections include protons from both elastic and inelastic breakup. The calculations agree well with the experimental data for the case of ^{27}Al although the calculations are shifted to slightly higher energies, probably due to the fact that their center-of-mass motion is not extracted correctly. This shift is much smaller in the case of ^{118}Sn. However, here the spectrum is underpredicted by about 20% at an angle of 9.5° and by a few percent at 13°. As the breakup at small scattering angles (corresponding to large impact parameters) is principally elastic, we suspect that more partial waves should be included in our elastic breakup calculation.
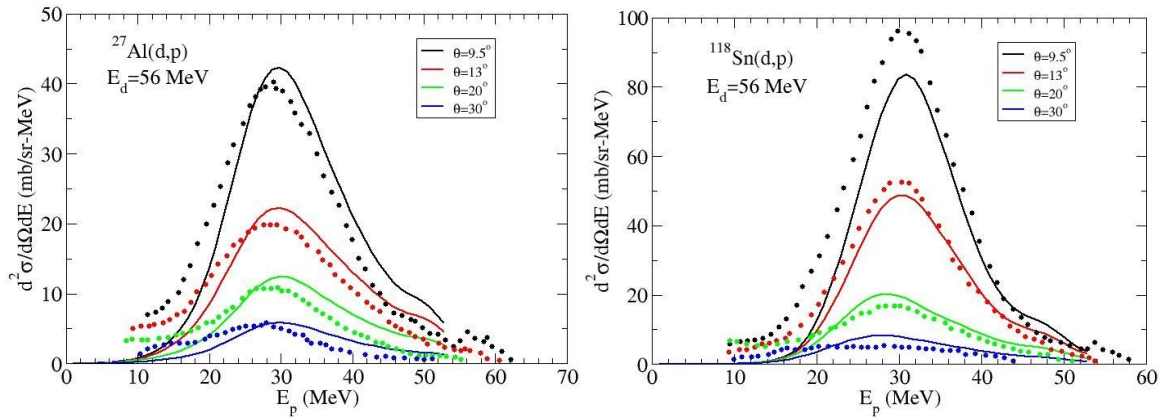

Fig. 2 (a) Inclusive double differential proton spectra for 56 MeV deuterons incident on ^{27}Al. (b) Inclusive double differential proton spectra for 56 MeV deuterons incident on ^{118}Si.
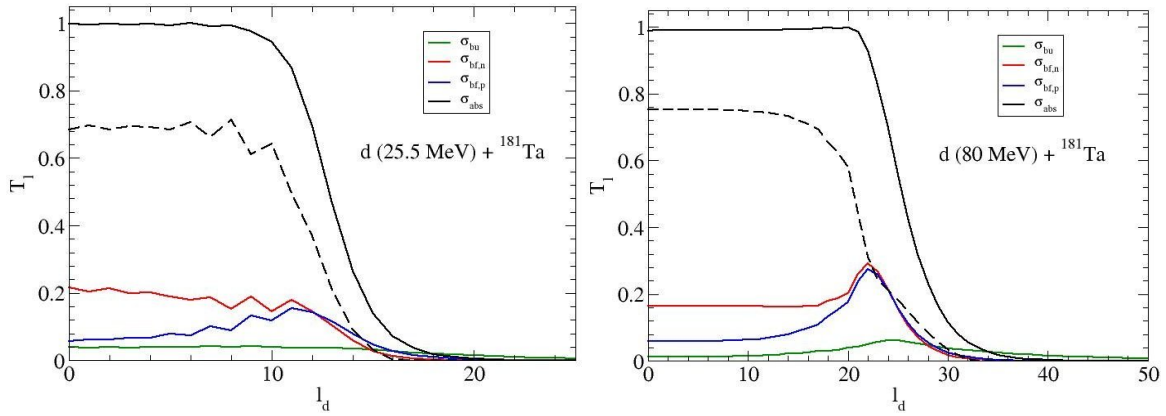
Fig. 3 (a) Reaction probabilities as a function of the deuteron angular momentum for 25.5 MeV deuterons incident on ^{48}Ti. (b) Reaction probabilities as a function of the deuteron angular momentum for 80 MeV deuterons incident on ^{181}Ta.

A standard optical model calculation of deuteron scattering furnishes a deuteron absorption probability (transmission coefficient) close to 1 below the grazing value of the angular momentum, corresponding to the solid black lines shown in Fig. 3 for deuterons incident at 25.5 and 80 MeV on ^{181}Ta. The flux lost due to elastic and inelastic breakup reduces this probability to about 75% for low partial waves in the nuclear interior and eliminates it in the surface region, as shown by the dashed lines in Fig. 3. Also shown are the neutron and proton absorption probabilities from inelastic breakup, which dominate in the surface region and extend into the nuclear interior with probabilities of about 10% and 20%, respectively. Only elastic breakup extends to higher angular momenta outside the range of the nuclear interaction.

A complete calculation of a deuteron-induced reaction must also take into account the formation and decay of the compound nucleus (CN) formed by absorption of the deuteron, as well as those formed by aborption of the neutrons or protons of inelastic breakup. The deuteron absorption cross section is determined by the subtracted transmission coefficients, shown as dashed lines in Fig. 3. The excitation energy of the CN that results is determined by the kinetic energy of the incident deuteron. Inelastic breakup reactions produce protons and neutrons over the entire kinematically allowed range of energy. The corresponding differential formation cross sections are thus distributions in energy and angular momentum. Two examples of these, for neutron and proton absorption due to inelastic breakup in deuteron-induced reactions at incident energies of 25.5 MeV and 80 MeV, respectively, are shown in Figs. 4 and 5.

In the reaction at 25.5 MeV, we observe in Fig. 4 that the neutron + target CN formation is well concentrated at lower energies while the proton + target CN formation is concentrated for the most part at higher energies, due to the importance of the Coulomb repulsion at this energy. The separation in energy of the neutron and proton distributions is still visible but much less distinct at 80 MeV, as can be seen in Fig. 5. At both
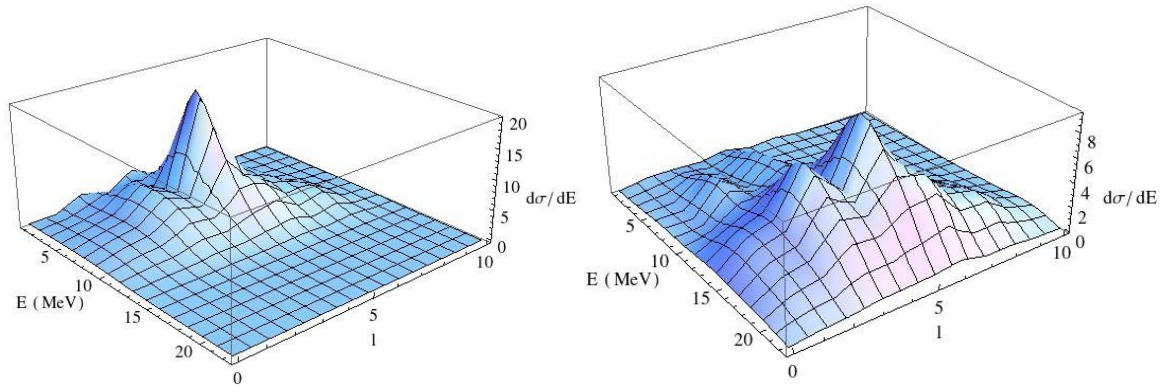

Fig. 4 (a) Energy - angular momentum distribution of neutron + target differential CN formation cross section for 25.5 MeV deuterons incident on ^{181}Ta. (b) Energy - angular momentum distribution of proton + target differential CN cross section formation for 25.5 MeV deuterons incident on ^{181}Ta.
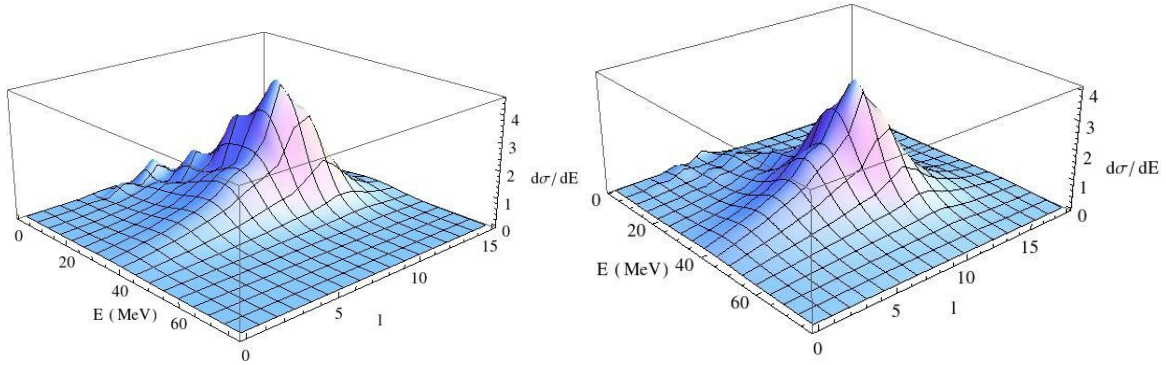
Fig. 5 (a) Energy - angular momentum distribution of neutron + target differential CN formation cross section for 80 MeV deuterons incident on ^{181}Ta. (b) Energy - angular momentum distribution of proton + target differential CN cross section formation for 80 MeV deuterons incident on ^{181}Ta.

incident energies, the proton + target distribution extends to larger values of the angular momentum, mainly due to the higher average energies of the protons that are absorbed.

Well-defined structures in energy and angular momentum appear in the differential cross sections at the lower incident deuteron energy of 25 Mev and, to a lesser extent, in the distributions at 80 MeV. These reactions should thus be used with care as surrogates to other reactions [2]. The compound nucleus formed could have an initial energy-angular momentum distribution very different from the one expected of a neutron- or proton-induced reaction.

4 Summary

We have used the post-form DWBA to calculate elastic and inelastic deuteron breakup cross sections in the zero-range limit. The breakup occurs for the most part outside the range of the nuclear interaction. However, the inelastic breakup cross sections, in which either the proton or neutron is absorbed by the target, are larger than the elastic one, in which the neutron and proton are simultaneously emitted.

The breakup reactions reduce deuteron absorption at small impact parameters by about 25% and dominate the surface region completely. The neutron + target absorption of inelastic breakup tends to occcur at lower energy than the proton + target one, due to Coulomb repulsion, which inhibits low-energy protons from entering the range of the nuclear interaction. The low-energy inelastic breakup CN formation cross sections are found to have well-defined structures in energy and angular momentum, which could have important consequences in reactions in which they are intended to serve as surrogates.

References

1. E. Betak et al, Technical Reports Series 473, Nuclear Data for the Production of Therapeutic Radionuclides, IAEA, Vienna, Austria, 2011, ISBN 978-92-0-115010-3.
2. J.E. Escher, J.T. Burke, F.S. Dietrich, N.D. Scielzo, I.J. Thompson, and W.Younes, Rev. Mod. Phys. **84**, 353 (2012).
3. G. Baur and D. Trautmann, Phys. Rep. **25**, 293 (1976).
4. G. Baur, F. Rösel, D. Trautmann and R. Shyam, Phys. Rep. **111**, 333 (1984).
5. A. Kasano and M. Ichimura, Phys. Lett. **B115**, 81 (1982).
6. N. Austern, Y. Iseri, M. Kamimura, M. Kawai, G. Rawitscher and M. Yahiro, Phys. Rep.**154**, 125 (1987).
7. P.J.A. Buttle and L.J.B. Goldfarb, Proc. Phys. Soc. **83**, 701 (1964).
8. A.J. Koning and J.P. Delaroche, Nucl. Phys. A **713** 231, (2003).
9. Y. Han, Y. Shi and Q. Shen, Phys. Rev. C **74**, 044615 (2006).
10. Haixia An and Chonghai Cai, Phys. Rev. C **73**, 054605 (2006).
11. C.M. Vincent and H.T. Fortune, Phys. Rev. C **2**, 782 (1970).
12. N. Matsuoka, M. Kondo, A. Shimizu, T. Saito, S. Nagamachi, H. Sakaguchi, A. Goto, F. Ohtani, Nucl. Phys. **A345**, 1 (1980).